DSCC2008-2249

IMAGE METHOD WITH DISTRIBUTED MULTIPOLE MODELS FOR ANALYZING PERMANENT-MAGNET-BASED ELECTROMAGNETIC ACTUATORS

Kok-Meng Lee
The George W. Woodruff School of
Mechanical Engineering
George Institute of Technology
Atlanta, GA 300332-0405
E-mail: kokmeng.lee@me.gatech.edu

Hungsun Son
Division of Intelligent Manufacturing
and Systems
Korea Institute of Machinery and
Materials (KIMM)
E-mail: hson@kimm.re.kr

Kun Bai
The George W. Woodruff School of
Mechanical Engineering
George Institute of Technology
Atlanta, GA 300332-0405
E-mail: kbai@gatech.edu

ABSTRACT

Many high-torque electromagnetic problems involve solving three dimensional (3D) magnetic fields of the permanent magnets (PMs) and/or electromagnet magnets (EMs) in the presence of magnetically conducting surfaces. This paper extends the distributed multi-pole (DMP) method, which offers a means to present the three-dimensional magnetic field solution in closed form, to account for the effects of the magnetic conducting boundary using an image method. We validate the DMP/image method by comparing the torques calculated using the Lorentz force equation and Maxwell stress tensor against numerical results computed using a finite element method (FEM). While two methods agree to within 5% in maximum torque, the DMP/image method takes less than 1% of the FEM computation time. With the numerically validated torque computation, we demonstrate how the DMP/image method can be used to analyze designs of a spherical wheel motor as illustrative practical applications.

NOMENCLATURE

Capitalized symbols		**Greek letter symbols**	
B	Flux density	Φ	Potential
D	Diameter	α, β, γ	XYZ Euler angles
H	Flux intensity	μ	relative
J	Current density vector	μ_o	Free space permeability
M_o	Magnetization vector	ρ	Circular loop radius
T	Torque	r, θ, ϕ	Spherical coordinates
Lowercase symbols			
a, p	Position vectors	l	Length of PM or EM
n	Surface normal vector	m	Strength of pole/dipole
g	Air gap		

INTRODUCTION

Actuators capable of delivering high torque with increasing accuracy, speed and dexterity are found in numerous applications such as manufacturing, robotics [1] and micro-factory [2]. Many of these high-torque electromagnetic applications involve solving the three dimensional (3D) magnetic fields of permanent and electro magnets in the presence of magnetically conducting surfaces.

Existing techniques for analyzing electromagnetic fields and designing multi-DOF PM-based actuators rely primarily on three approaches; namely, analytic solutions to Laplace's equation, numerical methods [3] and lumped-parameter analyses with some form of magnetic equivalent circuits [4]. However, these approaches have difficulties in achieving both accuracy and low computation time simultaneously, particularly when the fields involve magnetically conducting boundaries. These difficulties provided the motivation to develop new methods to derive closed-form field solutions for design and motion control of the actuators. In [5], we offer a relatively complete formulation, referred to here as the distributed multi poles (DMP) method, to model the magnetic fields of PMs and/or EMs in free space, and demonstrate its application to actuator, sensor and control applications in [6]. To account for the effects of magnetic conducting boundaries on the magnetic fields and torques, we explore the image method to reduce the problems to a more tractable form. As a basis problem-solving tool in electrostatics, the image method replaces the effects of the boundary on an applied field by adding or subtracting elementary fields behind the boundary line called image. The image method has commonly used for analyzing eddy current problems of electromagnetic fields; see for examples [7] [8]. The image method has also been used in FEM [9] to analyze unbounded magnetic fields containing ferromagnetic materials as well as in 2D analytical forms [10] in designing an electromagnetic actuator. Unlike [10] where solutions yield only

1

1st order accuracy, a nonlinear approach is used to account for effects of eddy currents with magnetic conducting boundary in [7]. However, the methods in [7] are mainly applicable for a simple structure of a conducive rod in a simplified geometry.

In this paper, we extend the DMP method to handle the magnetic conducting boundary using the image method.   The methods developed here offer a relatively complete solution of the magnetic field involving magnetic boundaries. Emphases are placed on spherical magnetic conducting boundary for design of multi-DOF spherical actuators.

The remainder of this paper offers the following:

1. We formulate a class of spherical actuator problems with magnetic boundary conditions that appear to be difficult to satisfy if the governing Poisson's or Laplace's equation is to be solved directly.   The conditions on the bounding surfaces in these problems are set up by appropriate image (equivalent) charges and solved using the image method.

2. To illustrate the procedure of the DMP/image method we model the magnetic field of a dipole (defined as a pair of source and sink with a separation) for three different magnetic boundaries; the dipole is (i) outside the magnetically grounded spherical rotor, (ii) inside a magnetically grounded hollow spherical stator, and (iii) in between a pair of spherical surfaces.   As will be shown, the magnetic field solutions formulated using the DMP model with the image method can be expressed in closed form.

3. We validate the DMP/image method by comparing the torques calculated using the Lorentz force equation and Maxwell stress tensor against numerical results computed using FEM, which agree to within 5% in maximum torque. As will be shown, the DMP/image method takes less than 1% of the FEM computation time.

4. With the numerically validated torque computation, we demonstrate how the DMP/image method can be used to study the effects of iron boundaries on the actuator design. For this, we compare the magnetic torque of electromagnetic pole designs, each with three different boundary conditions, and apply the DMP/image to analyze designs of a spherical wheel motor as illustrative practical applications.

SPHERICAL GROUNDED BOUNDARY

We consider here a class of electromagnetic problems where magnetic charges are in the presence of magnetically grounded conducting boundary.   Except at the point charges, the magnetic field is continuous and irrotational, for which a scalar potential Φ can then defined such that

$$\mathbf{H} = -\nabla\Phi \; ; \quad \mathbf{B} = \mu_0\mathbf{H} \qquad \text{(1a, b)}$$

where μ_0 is the permeability of free space. The formal approach for solving the magnetic field at every point outside the conducting boundary would be to solve the Laplace equation $\nabla^2\Phi = 0$, the solution to which must satisfy the following conditions. At points very close to the magnetic charge (source or sink), the potential Φ approaches that of the point charge alone

$$\Phi \to \pm m/(4\pi R) \text{ , as } R \to 0 \qquad \text{(2)}$$

where m is the strength of the magnetic charge; $+$ and $-$ signs designate that the pole is a source or a sink respectively; and R is the distance to $\pm m$. In addition, the potential is zero ($\Phi \to 0$) at the grounded conducting surface and points very far from $\pm m$.

Image Method of a Magnetic Charge

An alternative approach in lieu of a formal solution is the method of images, which replaces bounding surfaces by appropriate image charges, and the potential distributions can then be determined in a straightforward manner. As an illustration, consider Fig. 1(a) where the magnetic charge m (source or sink) in the free space is enclosed by the conducting spherical boundary (radius R) of very high permeability ($\mu \to \infty$, such as iron). The interest here is to determine the Φ distribution inside the grounded spherical surface due to the charge m.

(a) Magnetic charge and image   (b) Image of a dipole
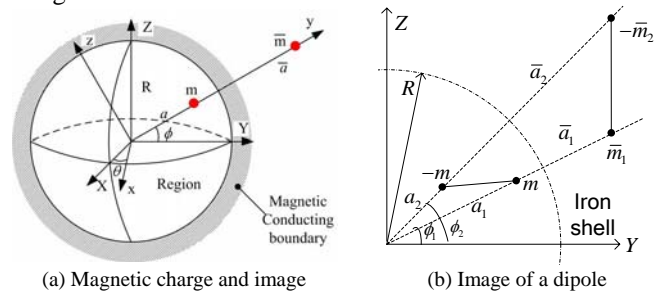
FIGURE 1. SPHERICAL MAGNETIC BOUNDARY

Without loss of generality, the surface is assigned a constant zero potential or $\Phi = 0$. In Fig. 1(a) where XYZ is the reference coordinate system, $\bar{m}$ is the image of the charge m and lies along the radial line connecting m. The image charge must be outside the region in which the field is to be determined, the parameters (m, a) and $(\bar{m}, \bar{a})$ are related by Eq. (3):

$$\bar{a}/R = -\bar{m}/m = \Lambda \quad \text{where } \Lambda = R/a . \qquad \text{(3)}$$

To facilitate the discussion, we define a local coordinate frame xyz such that m and $\bar{m}$ are on the y axis at the vector positions, $\mathbf{a}$ and $\bar{\mathbf{a}}$, respectively. In terms of spherical coordinates (r, θ, ϕ) , any point $\mathbf{x}(x,y,z)$ in the local frame can be expressed in the reference XYZ frame:

$$\mathbf{X}/|\mathbf{x}| = \begin{bmatrix} \cos\theta\cos\phi & \sin\theta\cos\phi & \sin\phi \end{bmatrix}^{\text{T}} \qquad \text{(4)}$$

Copyright © 2008 by ASME

where $\theta = \tan^{-1}(y/|\mathbf{x}|)$; and $\phi = \cos^{-1}(z/|\mathbf{x}|)$. Due to the symmetry of a sphere, the problem can be reduced to two dimensional (2D) in the yz plane. The potential at point $\mathbf{p}(x,y,z)$ for $0 \le p \le R$ where $p = |\mathbf{p}|$ is given by

$$\Phi(\mathbf{p}) = \frac{m}{4\pi}\left(\frac{1}{\sqrt{p^2 + a^2 - 2\mathbf{p}\cdot\mathbf{a}}} - \frac{1}{\sqrt{(p/\Lambda)^2 + R^2 - 2\mathbf{p}\cdot\mathbf{a}}} \right) \qquad (5)$$

$a = |\mathbf{a}|$; and $\bar{a} = |\bar{\mathbf{a}}|$. It can be seen from (5) that when $p=R$ (on spherical surface), Φ vanishes. The solution is exactly the same as that between two point charges m and $\bar{m}$ without the ground spherical boundary.

Images of a Magnetic Dipole

Since magnetic poles exist in pairs, we define a *dipole* as a pair of source m and sink $–m$ separated by a distance $\mathbf{d}$. For a dipole, the images of its source and sink (located at $\mathbf{a}_1$ and $\mathbf{a}_2$) are denoted as $\bar{m}_1$ and $-\bar{m}_2$ in Fig. 1(b). Using Eq. (3), the potential at $\mathbf{p}$ in the free space containing the dipole can be expressed as

$$\Phi(\mathbf{p}) = \frac{m}{4\pi}\left[\left(\frac{1}{|\mathbf{r}_1|} - \frac{\Lambda_1}{|\bar{\mathbf{r}}_1|} \right) - \left(\frac{1}{|\mathbf{r}_2|} - \frac{\Lambda_2}{|\bar{\mathbf{r}}_2|} \right) \right] \qquad (6)$$

where $\qquad \mathbf{r}_i = \mathbf{p} - \mathbf{a}_i$; $\quad \bar{\mathbf{r}}_i = \mathbf{p} - \bar{\mathbf{a}}_i$ $\qquad$ (7a,b)

$$\mathbf{a}_i / |\mathbf{a}_i| = \bar{\mathbf{a}}_i / |\bar{\mathbf{a}}_i| = \begin{bmatrix} 0 & \sin\phi_i & \cos\phi_i \end{bmatrix}^{\mathrm{T}} \qquad (8)$$

and $i = 1,2$ denote the source and sink respectively. In general, if $\mathbf{a}_1 \ne \mathbf{a}_2$, $\bar{m}_1 \ne \bar{m}_2$; as a result, the image source and sink of a dipole do not form a dipole, and do not satisfy the condition for continuous flow, $\nabla \cdot B = 0$. The solution of the image method is not valid in the magnetic conducting sphere since the image dipole does not actually exist but the images are rather standing in for the magnetic densities induced on the magnetic boundary.

Image Method for Spherical EM Actuator

For practical applications to be illustrated, we consider the following cases in spherical coordinates (r, θ, ϕ):

Case 1: The dipole m is outside the magnetically grounded spherical rotor of radius r_r, and its source and sink are located at $\mathbf{x}_{r1}$ and $\mathbf{x}_{r2}$ respectively:

$$\left| \bar{\mathbf{x}}_{ri} \right| / r_r = -\bar{m}_{ri}/m = \Lambda_{ri} \quad \text{where} \quad \Lambda_{ri} = r_r / |\mathbf{x}_{ri}| \qquad (9)$$

and $\quad \mathbf{x}_{ri}/|\mathbf{x}_{ri}| = \bar{\mathbf{x}}_{ri}/|\bar{\mathbf{x}}_{ri}| = \begin{bmatrix} \cos\theta_i \cos\phi_i & \sin\theta_i \cos\phi_i & \sin\phi_i \end{bmatrix}^{\mathrm{T}}$.

Case 2: The source and sink of the dipole m are inside the hollow magnetically grounded spherical stator of radius r_s, and located at $\mathbf{x}_{s1}$ and $\mathbf{x}_{s2}$ respectively.

$$\left| \bar{\mathbf{x}}_{sj} \right| / r_s = -\bar{m}_{sj}/m = \Lambda_{sj} \quad \text{where} \quad \Lambda_{sj} = r_s / |\mathbf{x}_{sj}| \qquad (10)$$

and $\quad \mathbf{x}_{sj}/|\mathbf{x}_{sj}| = \bar{\mathbf{x}}_{sj}/|\bar{\mathbf{x}}_{sj}| = \begin{bmatrix} \cos\theta_j \cos\phi_j & \sin\theta_j \cos\phi_j & \sin\phi_j \end{bmatrix}^{\mathrm{T}}$.

Case 3: The dipole m is in-between the grounded spherical rotor and stator, which are concentric. Each of the source and the sink will have two images located such that $\theta_i = \theta_j = \theta$ and $\phi_i = \phi_j = \phi$:

$$\bar{\mathbf{x}}_{ri}/|\bar{\mathbf{x}}_{ri}| = \bar{\mathbf{x}}_{sj}/|\bar{\mathbf{x}}_{sj}| = \begin{bmatrix} \cos\theta\cos\phi & \sin\theta\cos\phi & \sin\phi \end{bmatrix}^{\mathrm{T}} \qquad (11)$$

This is essentially a combination of Cases 1 and 2. Since the Laplace equation is linear, the solution can be obtained using the principle of superposition of Cases 1 and 2.

With the specified magnetic dipole and boundary, the images of the source and sink can be calculated from Eq. (9), Eq. (10) or Eq. (11), Φ and hence $\mathbf{H}$ in the free space can be found from Eq. (7) and Eq. (1) respectively.

ILLUSTRATIVE EXAMPLES

As an illustration, we consider the electromagnetic system (Fig. 2) which consists of two axially magnetized PMs on the spherical rotor, and an air-cored EM on the inside surface of the hollow spherical stator. The two PMs are identical but their magnetization vectors are in opposite directions (Fig. 2). The values of the parameters used in this simulation are given in Tab. 1.

TABLE 1. SYSTEM PARAMETERS*

Spheres	PM and its DMP model					EM
$r_r = 25.4$	$\ell_1 = 12.7$; $D_1 = 12.7$; $M_o = 1.34$T					$\ell_2 = 25.4$
$r_s = 63.5$	k	n	d/l	$2\rho/D_1$	m_k	$D_2 = 19.05$
$\delta_s = 26°$	0	1	0.264	0	-2.29	$D_3 = 9.525$
$\delta_r = 20°$	1	6	0.514	0.5	6.18	$N=1040$, $I= 4$A

* Dimensions in mm ; N= # of turns; and $m_k \times 10^{-5}$ in Am

The interest here is to investigate the effects of the iron boundaries on the magnetic field distribution (in the region between the rotor and stator surfaces) and on the torque acting on the rotor. For the purpose of deriving closed-form field solutions to facilitate the design and control of PM-based devices, we seek the field solutions outside the physical region of the magnet and magnetic boundary, particularly in the free space where the EM is located. Using the DMP method [5], we use k circular loops of n dipoles (strength m_k) evenly spaced on the circular loop of radius ρ and parallel to the magnetization vector to model the PM. The parameters characterizing the DMP model of the PM are summarized in Tab. 1. The corresponding images (location and strength) reflecting the source and sink of each dipole on the spherical boundaries can be derived from Eq. (6) with Eq. (9), Eq. (10) or Eq. (11).

3
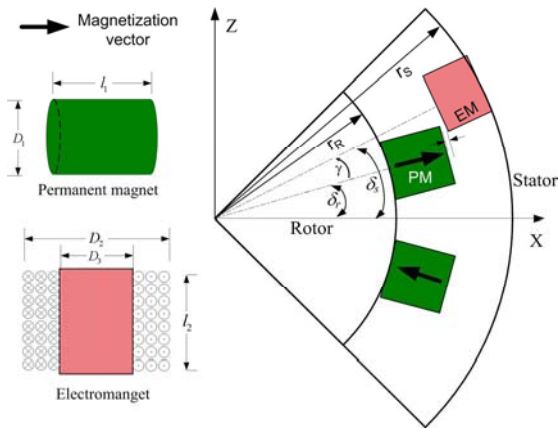
FIGURE 2. ACTUATOR SYSTEM WITH TWO PM'S AND EM

Figure 3 shows the magnetic field of the PM pair between two concentric magnetically grounded spheres when there is no current flowing through the air-core EM. To visually illustrate the image method, we graph the effects of image dipoles in the grounded spheres. It must be emphasized that the field distributions calculated using the image method are valid only in the free space between the spheres, and are invalid in the region $a<r_r$ & $a>r_s$ where Φ and **H** are zero in iron ($\mu\rightarrow\infty$) and are veiled in Fig. 3.
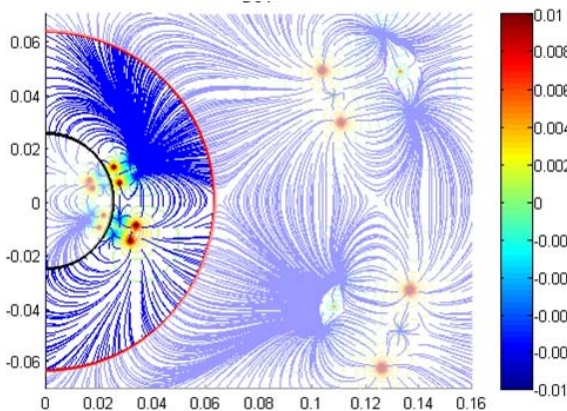
FIGURE 3. PM PAIR BETWEEN TWO MAGNETIC SURFACES

The effects of iron boundaries on the magnetic field distribution due to the pair of PMs are investigated by comparing four different design configurations (DCs):

  DC1: Rotor and stator are non-magnetic boundaries;
  DC2: Only the rotor is a magnetically conducting sphere.
  DC3: Only the stator is a magnetic conducting boundary.
  DC4: Both the rotor and stator are magnetic boundaries.

The simulated magnetic fields are compared in Fig. 4, where the bold solid circles indicate the spherical boundaries (black for the rotor and red for the stator). Figure 4(a), where there are no magnetic boundaries, serves as a basis for comparison. The effects of the iron rotor and stator boundaries on the magnetic field are compared in Fig. 4(b) and 4(c) respectively. As

expected, the magnetic field is perpendicular to magnetically grounded spherical surface ($\Phi=0$). Similarly, the combined effect of both the iron rotor and stator boundaries on the magnetically field I graphically displayed in Fig. 4(d).

EFFECTS OF IRON BOUNDARY ON THE TORQUE

Once the magnetic field is known, the torque acting on the rotor can be computed using the Lorentz force equation or Maxwell stress tensor, which are given in Annex A for completeness.

Numerical Validation

To validate the torque computed using the magnetic field computed from the DMP/image method, we compute the torque of the electromagnetic system shown in Fig. 5(a), where the values of the parameters are based on Tab. 1, and compare the results against the numerical method using ANSYS, a commercial finite-element (FE) analysis package.
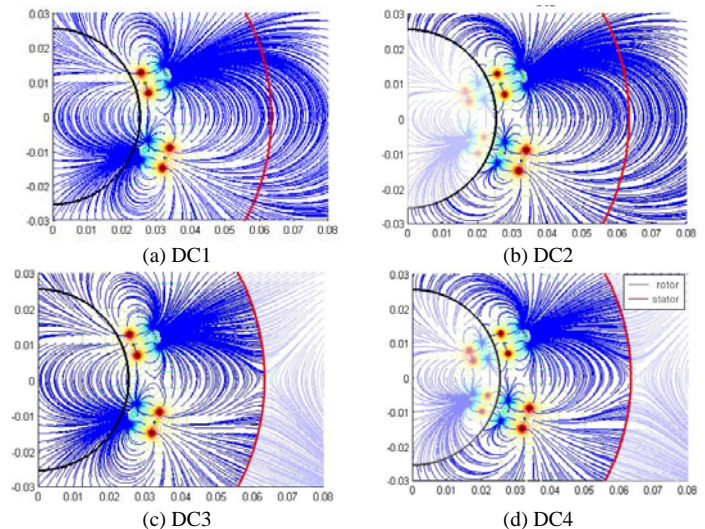
FIGURE 4. EFFECT OF BOUNDARIES ON MAGNETIC FIELD
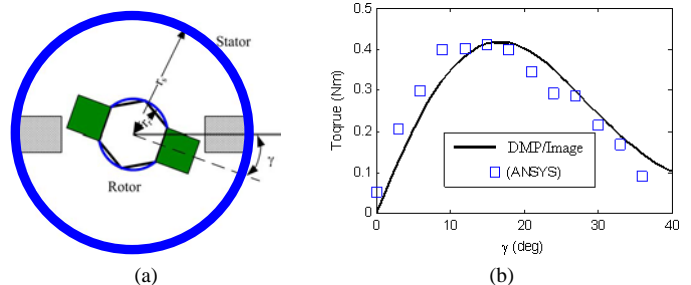
FIGURE 5. COMPARISONS OF COMPUTED TORQUES
Computational time: ANSYS=1,480seconds. DMP=17seconds

In Fig. 5(a), the rotor consisting of a pair of permanent magnets (PM) rotates with respect to two stator electromagnets (EM). Both the pairs of diagonally symmetric PM and EM are

4

mounted on spherical magnetic boundaries and on the same plane; in this study, the torque about the axis perpendicular to this plane is computed as a function of the separation angle γ.

ANSYS Model: Because of the symmetry, the FE model uses cylindrical iron boundaries for simplicity. The procedure for computing the electromagnetic torque using ANSYS can be found in [11] [12]. In ANSYS, the iron boundary was modeled using the eight-node SOLID96 elements (μ_r=1000 where μ_r is the relative permeability); the free space air volume was modeled using four-node INFIN47 elements; and the air-cored stator coil as SOURCE36 elements. For the PM $\mu_o \mu_r = B_r / H_c$ where B_r and H_c are the residual magnetization and the magnitude of coercive force vector respectively. In this computation, H_c=795,770A/m and B_r= 1.34T. With the total magnetic flux density obtained from ANSYS, the torque acting on the rotor is computed from Eq. (14) where Γ is a circular boundary enclosing the rotor with the pair of PMs.

Image Method with DMP Model: For the image method, the two concentric spherical boundaries along with the DMP model of the PM pair are employed in finding the images of the sources and sinks of the dipoles as discussed in Section III. With the specified multi-dipoles and the corresponding images, the magnetic field in the air space between the conducting surfaces is computed, which serves as a basis for computing the Lorentz force and hence the torque from Eq. (13).

The computed torque is compared in Fig. 5(b), which shows good agreement with a maximum error less than 5%. Using a Windows-based PC (dual core processor 2.21Ghz CPU and 1GB RAM), the image method with DMP model requires only 13 seconds to compute the torque curve while ANSYS requires 24.67 minutes to compute the thirteen data points. Some discrepancies occurred from the initial position. In the FE method, the quality of mesh significantly affects the accuracy of FE. The distortion of the automatically generated FE mesh could be the cause of the FE error (offset) even when the separation angle is zero.

Effects of Pole Design with Iron Boundary

With the numerically validated torque computation, we further examine the effects of iron boundaries on the actuator design by comparing the magnetic torque of the electromagnetic systems shown in Fig. 2 for a given stator radius r_s. Table 2 summarizes the specific geometries of the two designs respectively, where the differences are highlighted in **bold**; and g is the radial air-gap between the air-cored EM and rotor PMs. The values of the parameters that characterize the DMP models of the PM and EM are given in Tab. 3 and 4 respectively, where the % error is DMP modeling error defined along the magnetization axis of the PM:

$$\% \text{ error} = 100 \times \int_z |\Phi(z) - \Phi_A(z)| dz / \int_z |\Phi_A(z)| dz$$

TABLE 2. COMPARISON OF DESIGN PARAMETERS*

Spheres	Design A	Design B
r_r, r_s, g	**25.4**, 64.3, 0.76	**38.1**, 64.3, 0.76
PM: l_1, D_1, M_o	12.7, **17.78**, 1.34T	12.7, **19.05**, 1.34T
EM: l_2, D_2, D_3,	**25.4, 19.05, 9.525**	**19.05, 20.32, 7.62**
N, I	1040, 4A	1040, 4A

* Geometrical dimensions are in mm; N= # of turns

TABLE 3. DMP PARAMETERS OF PM (N=6)

Parameters	Design A (k=2)	Design B (k=1)
$m_j (\times 10^{-5})$, Am	4.95/0.1/12.59	-4.72/18.08
$\rho/(D_1/2)$	0.5	0.75
d/l	0.5162	0.3028
% error	3.3	3.6

TABLE 4. EQUIVALENT DMP PARAMETERS OF EM (N=6)

Parameters	Design A (k=1)	Design B (k=1)
$m_j (\times 10^{-8})$, Am	1.48\10.83	0.56 \ 5.48
d/l	0.9165	0.9501
% error	5.7	6.73

In each design, the torque is computed for four design configurations DC1 to DC4 (Fig. 2 and 4) and plotted as a function of the separation angle γ (between the magnetization axes of the PM and EM) in Fig. 6. In addition, the percentage increase in the maximum torques of DC2, DC3 and DC4 relative to DC1 are compared in Tab. 5.

Some observations are summarized as follows:

1. In Design A, the combined rotor/stator irons (DC4) contribute to 9.2% increase in the maximum torque; two-thirds are from the iron stator shell while one-third is from the iron rotor. The torque results are consistent with the predicted magnetic field distributions and can be explained with the aid of Fig. 3 as follows. Because of the infinitely high permeability of the iron, the magnetic fluxes go through the shortest path into the iron boundary perpendicularly. The shorter flux path implies higher magnetic field intensity, and thus has a direct effect to increase the force acting on the stator EM. In DC1, the path lines between the two PMs in the r_s region are much longer than those in the r_r region. As a result, the iron stator plays a more significant role in shortening the path lines than the iron rotor.

2. The image method with DMP model can be used to investigate the effect of pole designs *with iron boundaries* on the electromagnetic torque of a spherical wheel motor (SWM) [13]. Figure 7 compares the generated torque using the two different PM/EM pole designs (Tab. 2 and 3) for the structure shown in Fig. 5(a), where iron conductors were used in both the rotor and stator. The results show that Design B generates 58% larger maximum torque than Design A; both magnetic and mechanical structures contribute to this increase. Mechanically, Design B has a larger moment arm r_r while magnetically Design B has a smaller (r_s - r_r) air region between the rotor and stator

5

reducing magnetic flux leakages in the (r_s - r_r) region. In addition, the shortened EM which has an increased width for the same number of turns results in more current-conducting windings in the stronger magnetic fields.

TABLE 5. % INCREASE IN MAX.TORQUE RELATIVE TO DC1

Designs	DC2 (iron rotor)	DC3 (iron stator)	DC4 (both)
Design A	3.2 %	6.0 %	9.2 %
Design B	8.68 %	15.15 %	23.73 %

CONCLUSION

We extended the DMP method to a class of electromagnetic problems using the method image, where PMs and/or EMs are in the presence of magnetically grounded boundary. The DMP/Image method, which solves for the magnetic fields in closed form, has been validated by comparing the torques calculated using the Lorentz force equation against results computed using FEM with Maxwell stress tensor. While the comparison agrees to within 5% in maximum torque, the DMP/image method requires less than 1% of the FEM computation time. A relatively complete formulation has been presented for solving the magnetic field of the dipoles in three different cases of magnetically grounded surfaces. The image solutions have been applied to analyze designs of a spherical wheel motor as illustrative practical applications.

ACKNOWLEDGMENTS
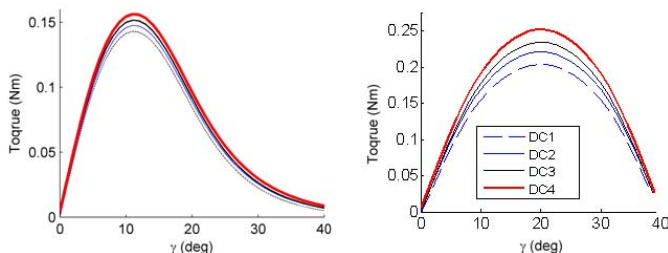
FIGURE 6. EFFECT OF IRON BOUNDARIES ON TORQUE
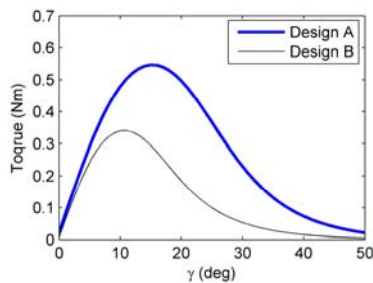
FIGURE 7. MAGNETIC FIELD AND TORQUE COMPARISON

REFERENCES

[1] S. Komada and K. Ohnishi, 1990. "Force feedback control of robot manipulator by the accelerationtracing orientation method", IEEE Trans. on Ind. Electronics, V. 37, pp. 6-12.

[2] D. Dornfeld, S. Min and Y. Takeuchi, 2006. "Recent Advances in Mechanical Micromaching," CIRP Annals-Manufacturing Tehcnology, vol. 55, pp. 745-768.

[3] K.-M. Lee, Q. Li, and H. Son, 2006. "Effects of numerical formulation on magnetic field computation using meshless methods," IEEE Trans. on Magnetics, V. 42, pp. 2164-2171.

[4] H. Ghoizad, M. Mirsalim, M. Mirzayee, and W. Cheng, 2007. "Coupled magnetic equivalent circuits and the analytical solution in the air-gap of squirrel cage induction machines," Int. J. of Applied Electromagnetics and Mechanics, vol. 25, pp. 749-754.

[5] K.-M. Lee and H. Son, 2007. "Distributed multipole model for design of permanent-magnet-based actuators," IEEE Trans. on Magnetics, V. 43, pp. 3904-3913.

[6] H. Son, and K.-M. Lee, 2008. "Distributed Multi-Pole Models for Design and Control of PM Actuators and Sensors," IEEE Trans. on Mechatronics, V. 13, pp. 228-238.

[7] K. Lee and K. Park, 2002. "Modeling eddy currents with boundary conditions by using Coulomb's law and the method of images," IEEE Trans. on Magnetics, V. 38, pp. 1333-1340.

[8] I. Dufour and D. Placko, 1996. "Original approach to Eddy current problems through a complex electrical image concept," IEEE Trans. on Magnetics, V. 32, pp. 348-365.

[9] Y. Saito, K. Takashi, and S. Hayano, 1988. "Finite element solution of unbounded magnetic field problem containing ferromagnetic materials," Vancouver, BC, pp. 2946-8.

[10] G. Xiong and S. A. Nasar, 1989. "Analysis of fields and forces in a permanent magnet linear synchronous machine based on the concept of magnetic charge," IEEE Trans. on Magnetics, V. 25, pp. 2713-2719.

[11] K.-M. Lee, R. A. Sosseh and Z. Wei, 2004. "Effects of the Torque Model on the Control of a VR Spherical Motor," IFAC J. of Control Engineering Practice, vol. 12/11 pp 1437-1449.

[12] K.-M. Lee, J. Joni, and H. Son, 2004. "Design Method for Prototyping a Cost-Effective Variable-Reluctance Spherical Motor (VRSM)," Proc. IEEE Conf. on Robotics, Automation and Mechatronics, Singapore, December 1-3.

[13] K.-M. Lee, H. Son, and J. Joni, 2005. "Concept Development and Design of a Spherical Wheel Motor (SWM)," Proc. of the IEEE ICRA, April 18-22, Barcelona, Spain, pp. 3652- 3657.

ANNEX A

TORQUE CALCULATION

The torque acting on the rotor can be computed using the Lorentz force equation:

$$\mathbf{T} = -\oint \mathbf{p} \times \mathbf{B} \times (I d\overline{\ell}\,) \text{ where } I = -\oiint \mathbf{J} \cdot d\mathbf{S} \qquad \text{(A.1)}$$

where $\overline{\ell}$ is the normalized current direction vector. In (A.1), the current density vector $\mathbf{J}$ is directly used in the calculation and thus, it is not necessary to compute the magnetic flux generated by the current loop. Thus, the Lorenz force calculation involves only modeling the $\mathbf{B}$-fields of the permanent magnets.

Alternatively, if the total $\mathbf{B}$ field (including both PM and EM) is known, the force on a body can also be computed from the surface integration in term of Maxwell stress tensor

$$\mathbf{T} = \frac{1}{\mu_0} \oint_\Gamma \mathbf{p} \times \left(\mathbf{B}(\mathbf{B} \cdot \mathbf{n}) - \frac{1}{2} B^2 \mathbf{n} \right) d\Gamma \qquad \text{(A.2)}$$

where Γ is an arbitrary boundary enclosing the body of interest; and $\mathbf{n}$ is the normal of the material interface.

7

Copyright © 2008 by ASME